nature geoscience

Article

https://doi.org/10.1038/s41561-023-01272-6

Elevated Grand Canyon groundwater recharge during the warm Early Holocene

Received: 21 July 2022

Accepted: 16 August 2023

Published online: 2 October 2023

Check for updates

Matthew S. Lachniet[1] ✉, Xiaojing Du[2], Sylvia G. Dee[2], Yemane Asmerom[3], Victor J. Polyak[3] & Benjamin W. Tobin[4]

Summer rainfall is an important contributor to water budgets in western North American deserts, where intense rainfall sustains ecosystems while also causing flash floods and damaging erosion. A better understanding of Grand Canyon palaeoclimate and the long-term history of the summer monsoon from summer-sensitive palaeoclimate records will improve our ability to project future hydroclimatic changes under warmer conditions. Here we show multi-proxy evidence for an intensification of the Early Holocene (11,700–8,200 years ago) hydrological cycle linked to a stronger and expanded summer North American Monsoon from calcite oxygen and uranium isotopes in a uranium-series precisely dated stalagmite from a Grand Canyon cave. Our results suggest that subsurface infiltration was greater in the Early Holocene than today at Grand Canyon. A data–model comparison with an isotope-enabled climate model suggests that enhanced infiltration was due to an Early Holocene monsoon intensification associated with rising atmospheric temperature. Projections of a future increase in precipitation intensity or more frequent and expanded North American monsoon rain events may paradoxically result in increased subsurface infiltration at Grand Canyon and other high-altitude plateaus, even within the context of western North American aridification in a hotter climate.

The North American Monsoon (NAM) is a regional-scale system of summer convection ranging from Central America to the southwestern United States[1–3] (Fig. 1). The response of NAM rainfall in the southwestern United States to future warming is uncertain, reflecting divergent model results[4]. For example, some studies suggested the NAM will intensify, but not necessarily with an increase in total summer precipitation[5,6], whereas others suggest a NAM weakening[7]. The intensification of summer rainfall events is a projected response to atmospheric warming from increased greenhouse gas concentrations[5,8]. There are distinct regional manifestations of the NAM[1,2]. Plateau heating draws moisture from the eastern Pacific Ocean to produce convection in the core monsoon region over the high terrain of the western Mexico ranges[1,9]. The southwestern United States, including the Grand Canyon region, represents the northern limit of the NAM, in a location that also receives winter synoptical-scale storms[1].

In this Article, we show oxygen stable-isotope and uranium geochemistry from a Grand Canyon cave stalagmite that documents an Early Holocene strengthening and expansion of NAM rainfall and cave infiltration, suggesting that aquifer recharge was enhanced during this past warm period. The Early and Middle Holocene are key time intervals for reconstructing hydroclimate and NAM history with palaeoclimatic data because of warmer-than-modern Northern Hemisphere temperatures[10,11] and the availability of proxy records sensitive to precipitation intensity, both of which document hydroclimatic changes in warm climates in the pre-instrumental record. The Grand Canyon of the Colorado River is an iconic landscape in western North America affected by the NAM and contains unique ecosystems and scenic value.

[1]Department of Geoscience, University of Nevada Las Vegas, Las Vegas, NV, USA. [2]Department of Earth, Environmental, and Planetary Sciences, Rice University, Houston, TX, USA. [3]Department of Earth and Planetary Sciences, University of New Mexico, Albuquerque, NM, USA. [4]Kentucky Geological Survey, Earth and Environmental Sciences, University of Kentucky, Lexington, KY, USA. ✉e-mail: Matthew.Lachniet@unlv.edu

https://doi.org/10.1038/s41561-023-01272-6

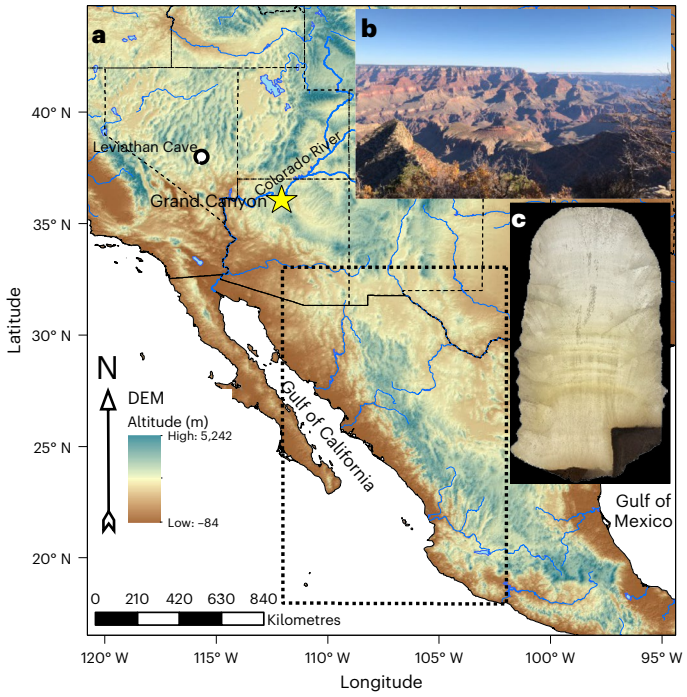

Fig. 1 | Site map of the NAM domain from Central America north through the southwestern United States. a, Digital elevation model (DEM) and site map. **b**, Grand Canyon landscape photograph **c**, Stalagmite GC-1. Speleothem palaeoclimate sites mentioned in the text are shown by white circles. The star shows the location for Grand Canyon iTRACE extraction at the cave site; the dashed black rectangle delineates the 'core' monsoon region used for the iTRACE extraction boundaries. Basemap from WorldClim v. 2.0 30 arcsec digital elevation model.

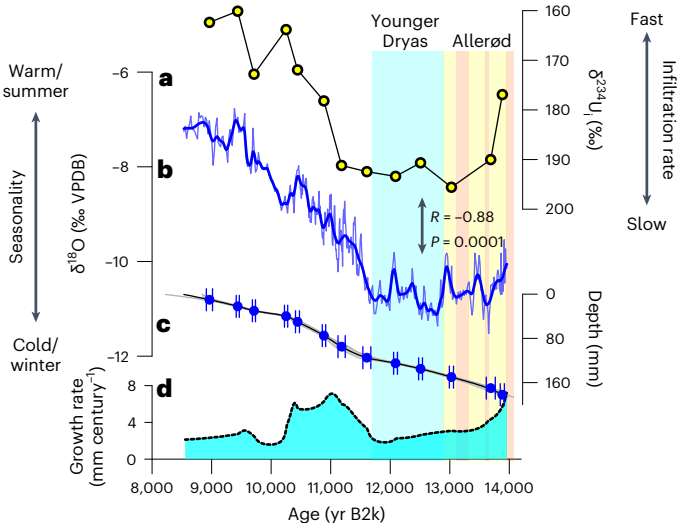

Fig. 2 | Grand Canyon stalagmite (GC-1) time-series data. a, $\delta^{234}U_i$; uncertainty is smaller than the symbols. **b**, $\delta^{18}O_c$. **c**, U-series age-depth model with ages and associated 2σ uncertainty; age model grey envelope indicates 95% confidence interval. **d**, The instantaneous growth rate from the age model. Coloured bars represent the Younger Dryas (light blue, coinciding with Greenland stadial 1) and Allerød intervals (pale yellow and orange, coinciding with Greenland interstadials 1a, b, c and d).

The Colorado Plateau, which is bisected by the Grand Canyon, is an important high-altitude plateau (~2,000 m; Fig. 1) that fosters summer monsoon convection[12] that is linked to sea surface temperatures exceeding 29.5 °C in the Gulf of California and advection of moist and warm air masses northward along the Colorado River valley[13]. During winter, storms from the mid- to high-latitude Pacific Ocean deliver rain and snow. Interannually, a reduction in plateau snow cover promotes the development of convection and monsoonal circulation the following summer[14,15]. Our speleothem record from the northern edge of the NAM should thus be sensitive to changes in the strength and geographic footprint of summer rainfall and to changes in the $\delta^{18}O$ values of precipitation ($\delta^{18}O_p$) and to cave infiltration.

Prolonged Early Holocene rise in $\delta^{18}O_c$ and infiltration

Conditions were sufficiently wet to sustain infiltration into the cave system and grow the Grand Canyon stalagmite GC-1 between ~13,960 and 8,530 years before 2000 CE (yr B2k), according to 13 precise (±25–75 yr) $^{230}Th/^{234}U$ disequilibrium dates (Supplementary Table 1 and Extended Data Fig. 1). At the end of the last glacial period, the stalagmite is characterized by calcite $\delta^{18}O$ values ($\delta^{18}O_c$) around −10 to −11‰ Vienna PeeDee Belemnite (VPDB) over the Allerød and Younger Dryas intervals[16] (Fig. 2), at which time the initial ^{234}U enrichment, shown as $\delta^{234}U_i$ (the ‰ deviation of the $^{234}U/^{238}U$ atomic ratio relative to the secular equilibrium value; Methods) was 190–195‰. During the Early Holocene, $\delta^{18}O_c$ gradually increased over three millennia to reach maximum values of −7‰ VPDB by ~8,600 yr B2k, which coincided with a decrease in $\delta^{234}U_i$ values to 160–180‰.

Stalagmite $\delta^{18}O_c$ variations in well-behaved stalagmites are a proxy for the $\delta^{18}O$ value of infiltrating water, which in turn relates to covariable moisture source, amount, precipitation phase (snow versus rain) and temperature changes of precipitation events. Because stalagmite GC-1 was not active, we are unable to assess whether modern $\delta^{18}O_c$ is in apparent equilibrium with drip-water $\delta^{18}O$. However, the GC-1 $\delta^{18}O_c$ time series replicates and is strongly correlated with the Leviathan Cave[17] stalagmite from the Great Basin ($r = 0.92$) and is anti-correlated to $\delta^{234}U_i$ ($r = -0.88$; Fig. 3), suggesting that the relative variations in GC-1 are robustly recording regional palaeoclimate variations (see the following).

The oxygen isotope values of precipitation in the southwestern United States are controlled by moisture source, atmospheric circulation[18], seasonality and temperature[17,19,20]. Long-term-amount effects in summer precipitation are not present[21,22], although convection is the dominant process in generating summer rainfall[23]. Summer precipitation on the Colorado Plateau is dominated by moisture delivered from the Gulf of California[23], with a lesser component of recycled moisture[22]. In general, moisture sources originating in the lower latitudes of the eastern Pacific Ocean have higher $\delta^{18}O_p$ and temperatures, whereas moisture masses originating from the high latitudes of the Pacific have lower $\delta^{18}O_p$ values and temperatures[17,19]. The $\delta^{18}O_p$ from Flagstaff, Arizona, 90 km south of the cave (Fig. 4), is positively correlated to monthly temperature ($r = 0.88$), related to both the changing moisture sources and the temperature of condensation[17,19,24]. Amount-weighted $\delta^{18}O_p$ values are −4.99‰ Vienna Standard Mean Ocean Water (VSMOW) for June–October and −10.43‰ VSMOW for November–May (Fig. 4). Co-varying temperature and moisture sources are the dominant control on $\delta^{18}O_p$ at our study site today, and they were probably dominant in the past.

Modern Grand Canyon cave-water $\delta^{18}O$ values are consistent with winter infiltration (Extended Data Fig. 2), and other observations confirm that summer rainfall today is not an important contributor to regional groundwater recharge[20,22,25,26]. Although cave drips were not active when we visited the cave, the $\delta^{18}O$ values of drips and pool waters ($n = 9$) from a nearby cave in Parashant National Monument (Methods) average −11.7 ± 0.25‰ VSMOW (Supplementary Table 2), overlapping the mean values of Grand Canyon springs of −11.9 ± 0.85‰ VSMOW[20], reflecting a dominant winter season for infiltration (Fig. 4).

To assess the potential controls on GC-1 $\delta^{18}O_c$, we first compare our stalagmite $\delta^{18}O_c$ with estimates of carbonate $\delta^{18}O$ deposited in apparent

https://doi.org/10.1038/s41561-023-01272-6

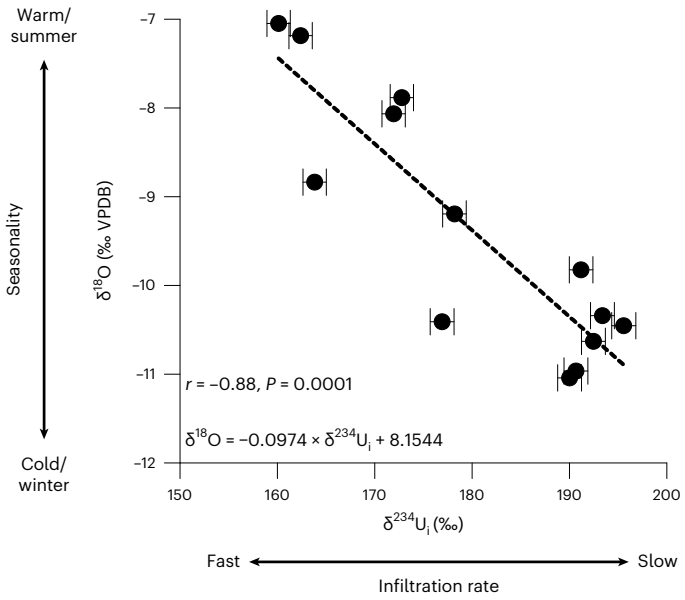

Fig. 3 | Correlation between $\delta^{18}O_c$ and $\delta^{234}U_i$ in stalagmite GC-1. The negative correlation suggests that periods with greater monsoon contribution (high $\delta^{18}O_c$) had shorter water–rock interaction times. $\delta^{234}U_i$ 2σ uncertainty is shown; uncertainty for $\delta^{18}O$ is ±0.08‰ and is smaller than the symbols.

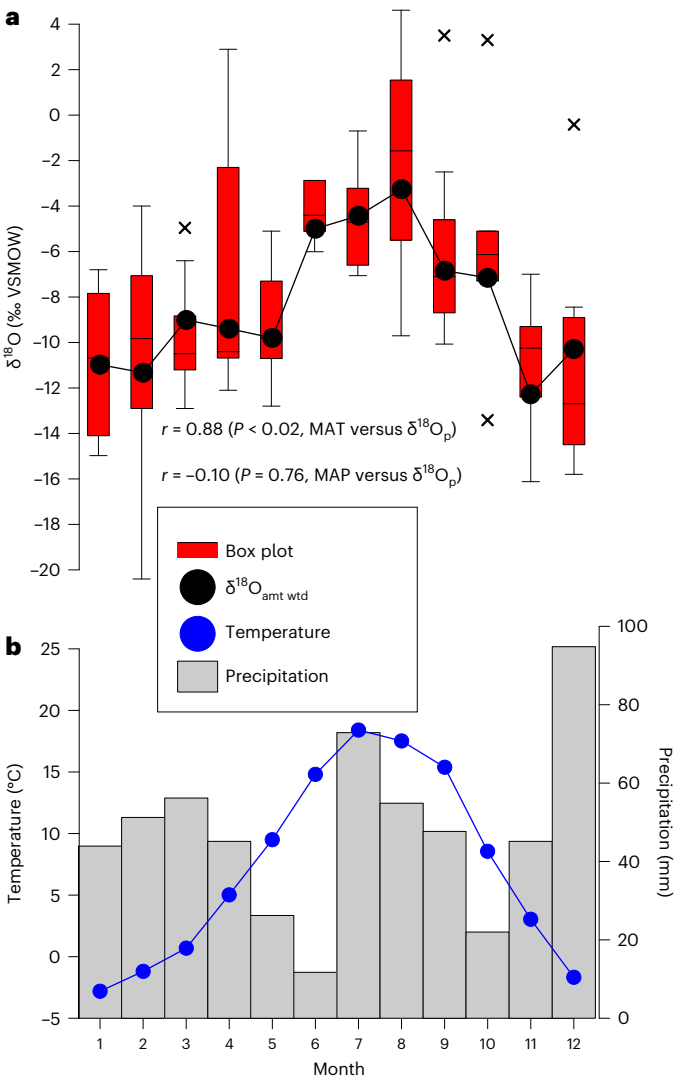

Fig. 4 | Modern stable-isotope and climate data from Flagstaff, Arizona. **a**, Box-and-whisker plots in red of monthly $\delta^{18}O$ at Flagstaff (box is defined by first and third quartiles; line is median; whiskers are maximum and minimum values; outliers are plotted as x), with precipitation amount-weighted $\delta^{18}O$ values ($\delta^{18}O_{amt\ wtd}$) shown in black circles and line (n = 97). **b**, Monthly temperature (blue) and precipitation (grey bars) of the Flagstaff data. In X-axis, the numbers 1–12 correspond to January–December. There is a clear seasonal cycle in monthly $\delta^{18}O$ values that is correlated to temperature and which is associated with the seasonal shift from winter westerly systems to the summer monsoon. MAT, mean annual temperature; MAP, mean annual precipitation. Data from ref. 51.

isotopic equilibrium with modern winter and summer precipitation, assuming, for simplicity, calcite precipitation at the modern cave temperature and seasonality of $\delta^{18}O_p$. Then we assess the potential for changing $\delta^{18}O_p$ to contribute to the observed $\delta^{18}O_c$ changes, using the isotope-enabled iTRACE simulation[27]. The $\delta^{18}O_c$ values in apparent isotopic equilibrium with Flagstaff, Arizona, summer and winter $\delta^{18}O_p$ at the modern cave temperature of 20.7 °C are −5.2 and −10.7‰ VPDB, respectively, using an empirical $\delta^{18}O$ fractionation factor between water and stalagmite calcite[28], or −4.8 and −10.2‰ VPDB, respectively, from an empirical fractionation factor for slow-growing calcites[29]. The GC-1 $\delta^{18}O_c$ time-series values (Fig. 2) of −10.5‰ VPDB during the Allerød and Younger Dryas intervals are most consistent with winter-season infiltration. The Early Holocene $\delta^{18}O_c$ values rose by 3.5‰ over three millennia from Younger Dryas levels to peak at −7.0‰ VPDB, a value intermediate between estimated modern winter (−10.2 to −10.7‰ VPDB) and summer (−4.8 to −5.2‰ VPDB) values. While some of the $\delta^{18}O_c$ increase could arise from more rain versus snow as temperatures increased above the freezing point during deglaciation, the highest $\delta^{18}O_c$ value of ~−7.0‰ VPDB is consistent with drip-water $\delta^{18}O$ of −6.8 to −7.3‰ VSMOW, a mix of modern summer and winter infiltration. For comparison, the highest monthly winter mean $\delta^{18}O_p$ at Flagstaff is −9.0‰ VSMOW in March (Fig. 4), about 2‰ lower than the estimated Early Holocene peak $\delta^{18}O$.

One explanation for the peak in $\delta^{18}O_c$ at ~8,600 yr B2k is an increase in the contribution of summer monsoon moisture to cave infiltration. This interpretation requires that Early Holocene summer infiltration was more important than now if past seasonal $\delta^{18}O_p$ was like today and contrasts with winter being the main season of modern infiltration into Grand Canyon aquifers[20,25,30]. Another interpretation is a large 2‰ increase in the $\delta^{18}O_p$ of infiltrating winter precipitation, a possibility that is without modern analogue but can be tested with the iTRACE output for the different boundary conditions of the Early Holocene. Moreover, the decrease in ^{234}U value, discussed in the following, is supportive of an overall increase in moisture, with greater contribution from a heavy $\delta^{18}O$ component, in this case, summer NAM.

In addition to the stalagmite evidence for higher $\delta^{18}O$ values of infiltration, we use multi-proxy data to asses an infiltration history using the initial calcite uranium isotope composition ($\delta^{234}U_i$), which is sensitive to epikarst and hydrologic processes[31], and $\delta^{13}C$ to assess changes in respired or soil CO_2 $\delta^{13}C$ values (Supplementary Tables 1 and 2 and Extended Data Fig. 6). It has been shown that $\delta^{234}U$ variability reflects the degree of water–rock interaction. In bedrock, ^{234}U is produced from the energetic α decay of ^{238}U via ^{234}Th and ^{234}Pa and, over time, fills damaged crystal lattice sites. Solution preferentially removes the ^{234}U relative to the bulk-rock uranium isotopes[32]. Dry intervals or low water–rock interaction permit ingrowth of ^{234}U in bedrock and result in higher drip-water $^{234}U/^{238}U$ and speleothem calcite[33,34], and vice versa for wet intervals, which more effectively remove ^{234}U. Because ^{234}U concentration in epikarst waters is a balance between production of ^{234}U and removal by water flux, drip-water ^{234}U should be inversely correlated to water flux through the epikarst to the first order[31,35]. The ingrowth of ^{234}U may take hundreds to thousands of years[36], but experimental data[37] and our results suggest that ^{234}U removal by water flux

https://doi.org/10.1038/s41561-023-01272-6

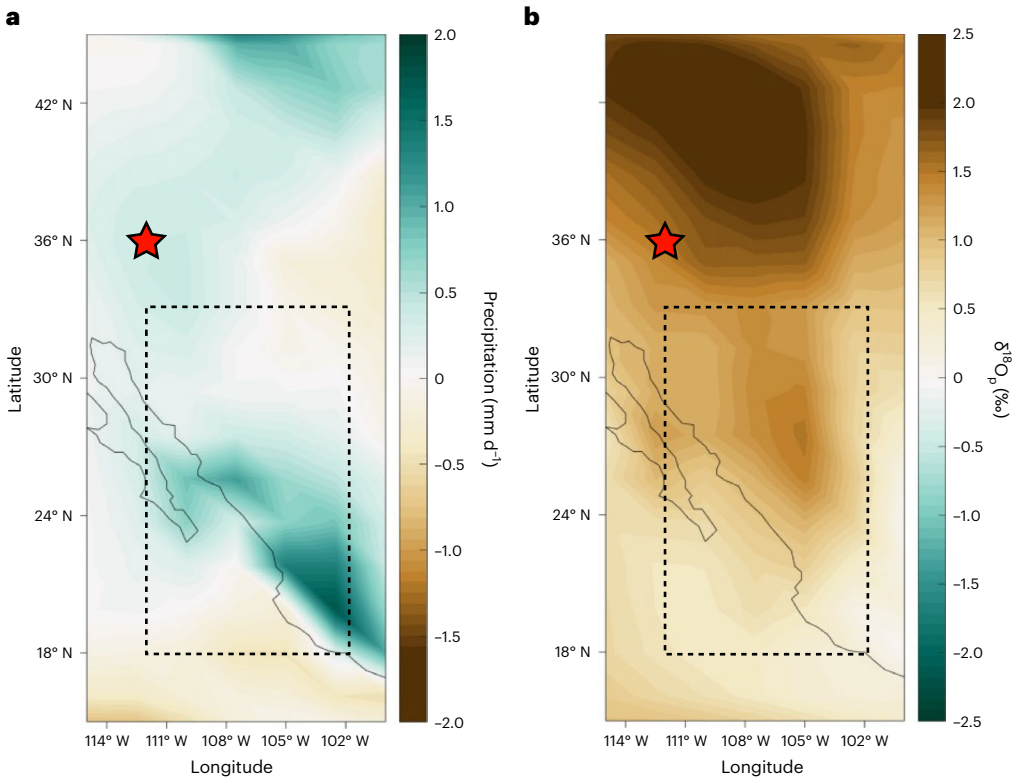

Fig. 5 | iTRACE model precipitation amount and $\delta^{18}O_p$ for 11 ka minus 14 ka. a,**b**, The iTRACE results show that June through August precipitation amount (**a**) and $\delta^{18}O_p$ (**b**) increased at 11 thousand years ago (ka) relative to 14 ka as the North American Monsoon intensified. Red star is GC-1 location.

happens on relatively short (<centennial) time scales (for example, a decrease in ~13‰ in ~300 years between 11,200 ± 61 and 10,904 ± 28 yr B2k in GC-1). We thus would anticipate some persistence in $\delta^{234}U_i$ over time, which lags climate changes, with a timescale of change that is possibly unique to each drip site within a cave.

The strong negative correlation ($r = -0.88$, $n = 13$) between $\delta^{18}O_c$ and $\delta^{234}U_i$ (Fig. 3) in stalagmite GC-1 supports a hydroclimatic control on water–rock interaction time and supports a climatic interpretation of $\delta^{18}O_c$. High $\delta^{234}U_i$ between 11,000 and ~14,000 yr B2k of >190‰ (Fig. 2) suggests slow infiltration rates in the epikarst. A single low value (180‰) at the beginning of the Allerød suggests somewhat wetter conditions at inception of stalagmite growth. An Early Holocene decrease in $\delta^{234}U_i$ (values <180‰) suggests greater water flux and coincides with an increasing stalagmite growth rate for the first millennia of the Early Holocene. Possible explanations for the high $\delta^{18}O_c$ and low $\delta^{234}U_i$ interval after 11,200 yr B2k include more intense monsoon precipitation and reduced water residence time or an increase in seasonal rainfall with higher $\delta^{18}O_p$ values. Stalagmite growth cessation at ~8,530 yr B2k followed a growth rate decrease and may relate to a warming threshold being crossed during peak temperatures, which coincides with the peak $\delta^{18}O_c$ in the Great Basin at Leviathan Cave[17], to drying[38] as evidenced by a paucity of stalagmite growth across the southwest at that time or to a switch in drip-water routing in the epikarst away from the GC-1 site.

Data–model comparison of the Early Holocene monsoon

Next, we use the iTRACE isotope-enabled simulations from 14,000 to 11,000 yr to compare with GC-1 $\delta^{18}O_c$. iTRACE[27] is a transient simulation of the Community Earth System Model (CESM v.1.3) that has water isotope physics explicitly embedded in the ocean, atmosphere, land surface and sea ice, reflecting an update to the original TRACE simulations of physical variables such as temperature and precipitation[39]. iTRACE is, at present, the only publicly available isotope-enabled transient simulation that spans this period. The key novelty is the simulation of $\delta^{18}O_p$ can be directly compared with speleothem data, providing a unique opportunity to test hypotheses of hydroclimate forcing.

iTRACE simulates the modern winter/summer bimodal rainfall peaks at Grand Canyon (Extended Data Fig. 3), as well as the zone of active rainfall in the core NAM region (Fig. 5). iTRACE also simulates an increase in both summer (June, July, August, September) precipitation and $\delta^{18}O_p$ from 14,000 to 11,000 yr B2k. Further, there was a weakening of the polar jet at 11,000 yr B2k with regional warming that was associated with a general increase in the $\delta^{18}O$ of water vapour across the tropical Pacific teleconnection pathway importing moisture towards the southwestern United States (Extended Data Fig. 4). Because the GC-1 $\delta^{18}O_p$ time series (the $\delta^{18}O_c$ record corrected for changes in temperature of ref. 40 and the equation of ref. 29) more closely approaches the summer $\delta^{18}O_p$ endmember at 11,000 yr B2k (Extended Data Fig. 5), the ~1.4‰ increase in GC-1 $\delta^{18}O$ is explained mainly by an increasing proportion of summer precipitation and further by a general increase in $\delta^{18}O_p$ of 1.2‰ in winter and 1.5‰ in summer. Together with the $\delta^{234}U_i$ evidence of enhanced aquifer infiltration after 11,000 yr B2k, the iTRACE data support the hypothesis of a NAM intensification and expansion to the Grand Canyon (Fig. 2). Although we cannot leverage the iTRACE $\delta^{18}O_p$ data after 11,000 yr B2k, the comparison of measured $\delta^{18}O_c$ with estimated modern winter and summer $\delta^{18}O_c$ from the Flagstaff precipitation data, the increase in summer $\delta^{18}O_p$ from iTRACE and the apparent increasing proportion of summer rainfall contribution after 11,000 yr B2k all support an intensification of the summer monsoon (Extended Data Fig. 5) that increased cave infiltration.

Gradual activation of the Early Holocene monsoon

Early Holocene hydroclimatic changes may be linked to orbital forcing and deglacial global boundary conditions. Speleothems from the Grand Canyon and Great Basin exhibit replicated gradual Early Holocene

https://doi.org/10.1038/s41561-023-01272-6

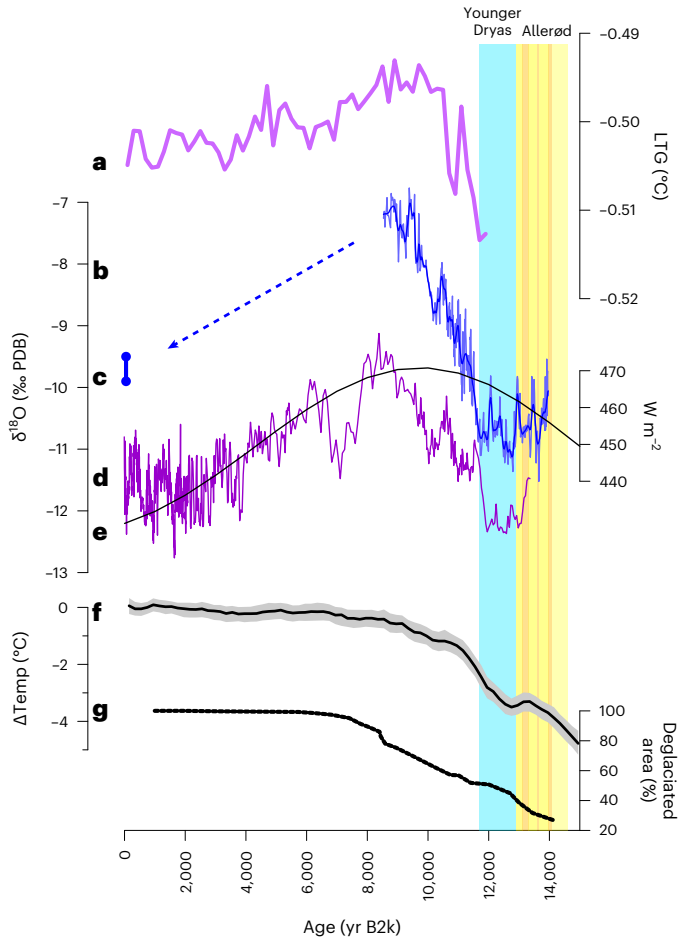

Fig. 6 | Palaeoclimate evolution of the western United States from speleothem, ice-sheet extent and model output. a, The reconstructed LTG of ref. 45; the LTG was calculated by subtracting binned composite temperatures at 50–90° N from those at 10° S to 30° N. **b**, The Grand Canyon speleothem $\delta^{18}O_c$ time series. The thick blue line is the mean COPRA (COnstructing Proxy Records from Age models) proxy output. **c**, Estimated modern $\delta^{18}O_c$ from drip waters. **d**, The Leviathan Cave $\delta^{18}O_c$ time series. **e**, July 21 insolation at 65° N. **f**, Global mean surface temperature reconstruction of ref. 40; grey envelope is 10th and 90th percentiles. **g**, The deglaciated area of ref. 43. The Grand Canyon and Great Basin speleothem records are plotted on the same *y* axis.

$\delta^{18}O_c$ increases that span three millennia (Fig. 6), a time interval that coincided with a humid period elsewhere in the southwest and Rocky Mountains[41,42]. The GC-1 stalagmite record is one of the most securely dated isotopic multi-proxy records for the entire southwest over this time interval, resulting from high-quality age dating due to pristine dense calcite. We emphasize that the replicated $\delta^{18}O_c$ increase in both the Grand Canyon and Great Basin stalagmites supports a regional climate signal in the stalagmite $\delta^{18}O$, and the higher $\delta^{18}O_c$ value at Grand Canyon compared with the Great Basin is consistent with a greater summer infiltration signal in the Arizona sector of the NAM compared with the Great Basin. Further, the replication between two sites in the southwest is strong evidence that non-equilibrium isotopic processes are not dominant controls on GC-1 $\delta^{18}O_c$ variation.

One hypothesis for the Early Holocene $\delta^{18}O_c$ increase is Laurentide ice-sheet retreat (Fig. 6)[43] and associated regional warming[40], which may have allowed for NAM strengthening[44] and the advection of moisture masses from the Gulf of California northwards. This process is similar to modern observations during periods when low areal snow cover facilitates monsoon convection[13]. Moreover, the differential warming of the high and low latitudes resulted in a reduced latitudinal temperature gradient (LTG) in the Early Holocene, which weakened the westerlies and winter storms[45], thus facilitating enhanced summer monsoon strength. A decrease in summer insolation after ~10,000 yr B2k was followed by a drop in Great Basin $\delta^{18}O_c$ and an increase in the LTG. Both the modern Leviathan Cave $\delta^{18}O_c$ and theoretical $\delta^{18}O_c$ precipitated from modern Grand Canyon cave waters have significantly lower values than those of the Early Holocene (Fig. 6). We infer that Grand Canyon $\delta^{18}O_c$ values also decreased over the Late Holocene, in line with data on southern Arizona speleothems[26,46], which show an insolation-controlled decrease in monsoon-derived cave infiltration.

On the basis of our multi-proxy palaeoclimate data and a comparison with the isotope-enabled iTRACE simulations, we conclude that there was a gradual intensification and incursion of the NAM over the Grand Canyon in the Early Holocene. This monsoon intensification was probably related to warming atmospheric temperatures associated with higher summer insolation, atmospheric warming, a reduced LTG and a decrease in snow and ice cover on the Colorado Plateau (Fig. 6). We further posit that these boundary conditions resulted in precipitation events sufficiently intense and frequent to infiltrate into the Grand Canyon cave (perhaps by increasing antecedent soil moisture[47]), despite having little ability to do so in today's climate. Although the single iTRACE model cannot be assumed to comprehensively assess all possible forcing scenarios during the Early Holocene and deglaciation, the data in hand are in strongest support for an Early Holocene monsoon intensification to explain the $\delta^{18}O_c$ and $\delta^{234}U_i$ time series in the Grand Canyon stalagmite. Additional high-quality monsoon records from the southwest region will further test this conclusion.

Implication of aquifer recharge in warm climates

The documentation of increased infiltration during the Early Holocene has implications for future climate change in the Grand Canyon region. More intense rainfall events are projected in response to a warmer atmosphere[5,8]. A past increase in the intensity of precipitation may not, however, have led to greater mean summer or mean annual precipitation because the frequency of such events may have decreased[8]. While the Early Holocene is not a direct analogue for future climate, our data do suggest that warm-season groundwater infiltration may vary as a function of precipitation intensity, at least for the high-altitude Colorado Plateau region. For example, future warming is projected to increase the intensity of extreme rainfall events, with up to a doubling in the future with a high-end emissions scenario[5], even while having little change or even reductions in North American Monsoon rainfall totals[8,48]. Against the context of increasing drought and aridity forced by rising atmospheric temperatures in western North America[48], rising heat extremes[49] and increasingly potent fire conditions[50], a future increase in NAM rainfall intensity may paradoxically increase cave infiltration at Grand Canyon in the future. The potential response of infiltration to warmer conditions in the hotter low-altitude southwestern deserts remains to be tested. Aside from supporting the idea that the NAM strengthened during the last deglaciation, our data show that aquifer infiltration at Grand Canyon may have also increased at that time, with implications for further recharge in projected warmer climates.

Online content

Any methods, additional references, Nature Portfolio reporting summaries, source data, extended data, supplementary information, acknowledgements, peer review information; details of author contributions and competing interests; and statements of data and code availability are available at https://doi.org/10.1038/s41561-023-01272-6.

References

1. Metcalfe, S. E., Barron, J. A. & Davies, S. J. The Holocene history of the North American Monsoon: 'known knowns' and 'known unknowns' in understanding its spatial and temporal complexity. *Quat. Sci. Rev.* **120**, 1–27 (2015).

2. Higgins, R. W., Chen, Y. & Douglas, A. V. Interannual variability of the North American warm season precipitation regime. *J. Clim.* **12**, 653–680 (1999).
3. Bernal, J. P. et al. A speleothem record of Holocene climate variability from southwestern Mexico. *Quat. Res.* **75**, 104–113 (2011).
4. Brierley, C. M. et al. Large-scale features and evaluation of the PMIP4–CMIP6 mid Holocene simulations. *Climate* **16**, 1847–1872 (2020).
5. Seneviratne, S. I. et al. in *Climate Change 2021: The Physical Science Basis* (eds Masson-Delmotte, V. et al.) 1513–1766 (Cambridge Univ. Press, 2021).
6. Asmerom, Y., Polyak, V., Rasmussen, J. B., Burns, S. & Lachniet, M. S. Multidecadal to multicentury scale collapses of Northern Hemisphere monsoons over the past millennium. *Proc. Natl Acad. Sci. USA* **110**, 9651–9656 (2013).
7. Pascale, S. et al. Weakening of the North American monsoon with global warming. *Nat. Clim. Change* **7**, 806–812 (2017).
8. Thackeray, C. W., Hall, A., Norris, J. & Chen, D. Constraining the increased frequency of global precipitation extremes under warming. *Nat. Clim. Change* **12**, 441–448 (2022).
9. Liebmann, B. et al. Characteristics of North American monsoon summertime rainfall with emphasis on the Monsoon. *J. Clim.* **21**, 1277–1294 (2008).
10. Kaufman, D. et al. Holocene global mean surface temperature, a multi-method reconstruction approach. *Sci. Data* **7**, 201 (2020).
11. Thompson Alexander, J., Zhu, J., Poulsen Christopher, J., Tierney Jessica, E. & Skinner Christopher, B. Northern Hemisphere vegetation change drives a Holocene thermal maximum. *Sci. Adv.* **8**, eabj6535 (2022).
12. Anderson, R. S., Betancourt, J. L., Mead, J. I., Hevly, R. H. & Adam, D. P. Middle- and late-Wisconsin paleobotanic and paleoclimatic records from the southern Colorado Plateau, USA. *Palaeogeogr. Palaeoclimatol. Palaeoecol.* **155**, 31–57 (2000).
13. Erfani, E. & Mitchell, D. L. A partial mechanistic understanding of the North American monsoon. *J. Geophys. Res. Atmos.* **119**, 13096–13115 (2014).
14. Notaro, M. & Zarrin, A. Sensitivity of the North American Monsoon to antecedent Rocky Mountain snowpack. *Geophys. Res. Lett.* **38**, L17403 (2011).
15. Gutzler, D. S. Covariability of spring snowpack and summer rainfall across the southwest United States. *J. Clim.* **13**, 4018–4027 (2000).
16. Rasmussen, S. O. et al. A new Greenland ice core chronology for the last glacial termination. *J. Geophys. Res. Atmos.* **111**, D06102 (2006).
17. Lachniet, M. S., Asmerom, Y., Polyak, V. & Denniston, R. Great basin paleoclimate and aridity linked to Arctic warming and tropical Pacific sea surface temperatures. *Paleoceanogr. Paleoclimatol.* **35**, e2019PA003785 (2020).
18. Liu, Z., Kennedy, C. D. & Bowen, G. J. Pacific/North American teleconnection controls on precipitation isotope ratios across the contiguous United States. *Earth Planet. Sci. Lett.* **310**, 319–326 (2011).
19. Friedman, I. Stable isotope composition of waters in the Great Basin, United States 1. Air-mass trajectories. *J. Geophys. Res.* **107**, ACL-14 (2002).
20. Solder, J. E. & Beisner, K. R. Critical evaluation of stable isotope mixing end-members for estimating groundwater recharge sources: case study from the South Rim of the Grand Canyon, Arizona, USA. *Hydrol. J.* **28**, 1575–1591 (2020).
21. Eastoe, C. J. & Dettman, D. L. Isotope amount effects in hydrologic and climate reconstructions of monsoon climates: implications of some long-term data sets for precipitation. *Chem. Geol.* **430**, 78–89 (2016).
22. Tulley-Cordova, C. L., Putman, A. L. & Bowen, G. J. Stable isotopes in precipitation and meteoric water: sourcing and tracing the North American Monsoon in Arizona, New Mexico, and Utah. *Water Resour. Res.* **57**, e2021WR030039 (2021).
23. Jana, S., Rajagopalan, B., Alexander, M. A. & Ray, A. J. Understanding the dominant sources and tracks of moisture for summer rainfall in the southwest United States. *J. Geophys. Res. Atmos.* **123**, 4850–4870 (2018).
24. Coplen, T. B. et al. Extreme changes in stable hydrogen isotopes and precipitation characteristics in a landfalling Pacific storm. *Geophys. Res. Lett.* **35**, L21808 (2008).
25. Tobin, B. W., Springer, A. E., Kreamer, D. K. & Schenk, E. Review: the distribution, flow, and quality of Grand Canyon Springs, Arizona (USA). *Hydrol. J.* **26**, 721–732 (2018).
26. Truebe, S. A. *Past Climate, Modern Caves, and Future Resource Management in Speleothem Paleoclimatology*. PhD thesis, Univ. Arizona (2016).
27. He, C. et al. Deglacial variability of South China hydroclimate heavily contributed by autumn rainfall. *Nat. Commun.* **12**, 5875 (2021).
28. Tremaine, D. M., Froelich, P. N. & Wang, Y. Speleothem calcite farmed in situ: modern calibration of $\delta^{18}O$ and $\delta^{13}C$ paleoclimate proxies in a continuously-monitored natural cave system. *Geochim. Cosmochim. Acta* **75**, 4929–4950 (2011).
29. Daëron, M. et al. Most Earth-surface calcites precipitate out of isotopic equilibrium. *Nat. Commun.* **10**, 429 (2019).
30. Bills, D. J., Flynn, M. E. & Monroe, S. A. Hydrogeology of the Coconino Plateau and Adjacent Areas, Coconino and Yavapai Counties, Arizona, (ed US Geological Survey Department of the Interior) 101 (US Geological Survey, 2007).
31. Zhou, J. et al. Geochemistry of speleothem records from southern Illinois: development of $(^{234}U)/(^{238}U)$ as a proxy for paleoprecipitation. *Chem. Geol.* **221**, 1–20 (2005).
32. Kigoshi, K. Alpha-recoil thorium-234: dissolution into water and the uranium-234/uranium-238 disequilibrium in nature. *Science* **173**, 47–48 (1971).
33. Polyak, V., Asmerom, Y., Burns, S. & Lachniet, M. S. Climatic backdrop to the terminal Pleistocene extinction of North American mammals. *Geology* **40**, 1023–1026 (2012).
34. Plagnes, V., Causse, C., Genty, D., Paterne, M. & Blamart, D. A discontinuous climatic record from 187 to 74 ka from a speleothem of the Clamouse Cave (south of France). *Earth Planet. Sci. Lett.* **201**, 87–103 (2002).
35. Robinson, L. F., Henderson Gideon, M., Hall, L. & Matthews, I. Climatic control of riverine and seawater uranium-isotope ratios. *Science* **305**, 851–854 (2004).
36. Rasilainen, K., Nordman, H., Suksi, J. & Marcos, N. Direct alpha-recoil as a process to generate U-234/U-238 disequilibrium in groundwater. *MRS Online Proc. Libr.* **932**, 4.1 (2006).
37. Fleischer, R. L. Isotopic disequilibrium of uranium: alpha-recoil damage and preferential solution effects. *Science* **207**, 979–981 (1980).
38. Polyak, V. J. & Asmerom, Y. Orbital control of long-term moisture in the southwestern USA. *Geophys. Res. Lett.* **32**, L19709 (2005).
39. He, F. *Simulating Transient Climate Evolution of the Last Deglaciation with CCSM3*. PhD thesis, Univ. Wisconsin Madison (2011).
40. Osman, M. B. et al. Globally resolved surface temperatures since the Last Glacial Maximum. *Nature* **599**, 239–244 (2021).
41. Shuman, B. N. & Serravezza, M. Patterns of hydroclimatic change in the Rocky Mountains and surrounding regions since the Last Glacial Maximum. *Quat. Sci. Rev.* **173**, 58–77 (2017).

42. Weng, C. & Jackson, S. T. Late Glacial and Holocene vegetation history and paleoclimate of the Kaibab Plateau, Arizona. *Palaeogeogr. Palaeoclimatol. Palaeoecol.* **153**, 179–201 (1999).
43. Dyke, A. S. An outline of North American deglaciation with emphasis on central and northern Canada. In *Quaternary Glaciations—Extent and Chronology: Part II: North America* (eds Ehlers, J. & Gibbard, P. L.) 373–424 (Elsevier, 2004).
44. Bhattacharya, T., Tierney, J. E., Addison, J. A. & Murray, J. W. Ice-sheet modulation of deglacial North American monsoon intensification. *Nat. Geosci.* **11**, 848–852 (2018).
45. Routson, C. C. et al. Mid-latitude net precipitation decreased with Arctic warming during the Holocene. *Nature* **568**, 83–87 (2019).
46. Cole, J. E. et al. A Continuous Holocene Record of Hydroclimate from Kartchner Cavern, AZ, Supported by Multiyear Dripwater Monitoring, In *Proc. American Geophysical Union Annual Meeting* (2017).
47. Jasechko, S. & Taylor, R. G. Intensive rainfall recharges tropical groundwaters. *Environ. Res. Lett.* **10**, 124015 (2015).
48. Douville, H. et al. In *Climate Change 2021: The Physical Science Basis* (eds Masson-Delmotte, V. et al.) 1055–1210 (Cambridge Univ. Press, 2021).
49. Thompson, V. et al. The 2021 western North America heat wave among the most extreme events ever recorded globally. *Sci. Adv.* **8**, eabm6860 (2022).
50. Iglesias, V., Balch Jennifer, K. & Travis William, R. US fires became larger, more frequent, and more widespread in the 2000s. *Sci. Adv.* **8**, eabc0020 (2022).
51. IAEA/WMO (International Atomic Energy Agency/World Meteorological Organization, 1998); https://nucleus.iaea.org/wiser/index.aspx

Methods

We collected stalagmite GC-1 from a cave in the Redwall Formation[52] on the South Rim of eastern Grand Canyon in October of 2017. Because of the sensitive nature of the cave location, its geographic coordinates are being withheld; coordinates for Grand Canyon National Park headquarters are 36.055° N, 112.140° W, 2,093 m above sea level. Interested parties may apply to the National Park Service at Grand Canyon National Park for more information. The cave is structurally controlled, with passages following local faulting patterns. Caves in the Redwall limestone typically follow these local to regional structural patterns[53]. The sample site in the cave is located at an elevation of 1,462 m and 550 m from the nearest entrance in a side passage beyond a constriction, which limits atmospheric exchange with the outside environment. The sampled stalagmite is in an area with the highest concentration of epigenic speleothems in the cave, which is proximal to a small surface drainage as it crosses onto the limestone. In other caves in the Grand Canyon and elsewhere, this has been suggested to represent a zone of concentrated recharge[54]. While regionally, the Redwall limestone has upwards of 1,000 m of overlying sedimentary units, the sample site is overlain by ~35 m of Redwall limestone with all other overlying units eroded away above the cave. Infiltration is restricted to precipitation that falls on the overlying land surface and not to regional flow. The 187-mm-tall stalagmite GC-1 was collected in growth position from atop breakdown and is composed of dense translucent calcite (Fig. 1).

Drips in the cave were too slow to sample during the visit. One pool-water sample was collected for stable isotopes in a 2 ml glass vial on the October 2017 cave visit and stored at room temperature until analysis on 12 June 2020. The pool water had a $\delta^{18}O$ value of −9.7‰ VSMOW and a low deuterium excess value of −1.1, indicating evaporation before analysis. We suspect that the rubber septa and cap did not prevent evaporation of the sample over the 27-month interval between collection and analysis, so we favour use of the $\delta^{18}O$ values of drip waters from the nearby Parashant cave 3504 for comparison with the stalagmite data. Active stalagmites were not available for sampling for cave conservation reasons.

We completed 13 $^{230}Th/^{234}U$ disequilibrium dates at the Radiogenic Isotope Laboratory at the University of New Mexico by drilling along stratigraphic layers (Supplementary Table 1). Ages are reported in years before the year 2000 CE (yr B2k) and were determined on the updated decay constants for ^{234}U and ^{230}Th (ref. 55). Stalagmite GC-1 grew continuously for ~5,430 years between ~13,960 yr B2k and 8,530 yr B2k, spanning the North Atlantic climate intervals of the Allerød, Younger Dryas and Early Holocene intervals. Measured $\delta^{234}U$ is defined as $\delta^{234}U = ([^{234}U/^{238}U]_{activity} - 1) \times 1{,}000$, and $\delta^{234}U_i$ is calculated from the radiogenic ingrowth from the sample's $^{230}Th/^{234}U$ age: $\delta^{234}U_i = \delta^{234}U_{measured} \times e^{\lambda 234 \times T}$, where λ_{234} is the decay constant of ^{234}U (ref. 55). The precise U-series ages are due to the high ^{238}U concentrations (~1–4 ppm) and $\delta^{234}U_i$ values of +160–200‰, resulting in age model uncertainty mostly between 50 and 150 years at the 95% confidence interval (Extended Data Fig. 1).

We drilled 373 carbonate powders for $\delta^{18}O$ and $\delta^{13}C$ values at 0.5 mm resolution on a micromill with a 0.508 mm diameter drill bit and analysed the powders on a Kiel IV automated carbonate preparation device coupled in dual inlet mode to a Delta V Plus mass spectrometer via phosphoric acid reaction at 70 °C. Repeated measurements of an internal calcite standard (USC-1) yields precisions of ±0.04 and 0.07 ($n = 63$) for $\delta^{13}C$ and $\delta^{18}O$, respectively. Age modelling was done with the COPRA algorithm[56] using a cubic polynomial, which estimates age uncertainties over time, and a time-exact estimate of the $\delta^{13}C$ and $\delta^{18}O$ values. The isotope sampling resolution is typically better than 20 years between samples, and each isotope sub-sample integrates between 8 and 20 years of growth, allowing a high-resolution investigation of sub-centennial-scale climate variability (Extended Data Fig. 1).

Water stable-isotope values were determined via analysis with a ThermoElectron high-temperature thermal conversion elemental analyser by reacting the sample at 1,400 °C in the presence of ultra-high-purity helium and glassy carbon via a bottom-flow adaptor. CO and H_2 were separated on a gas chromatograph column and analysed in continuous flow mode via a ConFlo III interface to the Delta V Pluss mass spectrometer. Precision was ±0.2‰ and 2.0‰ for $\delta^{18}O$ and $\delta^{2}H$, respectively.

We compiled precipitation stable-isotope data from Flagstaff, Arizona, from the Global Network for Isotopes in precipitation[51] network to aid in interpretation of the stalagmite $\delta^{18}O$ data. We calculated weighted summer (June–October) and winter (November–May) precipitation $\delta^{18}O$ values. Flagstaff (35.19° N, 111.60° W, 2,400 m) is located ~100 km south of the study area. Cave drip waters plot on the local meteoric water line (Extended Data Fig. 2).

Cave climate was monitored with a HOBO data logger for temperature and relative humidity for ~16 months (30 December 2015 to 26 March 2017) at 30-minute intervals. Cave climate measurements near the sample site indicated constant 100% relative humidity (continuous logging between January 2016 and April 2017) and our site visit (October 2017). Logger temperature was relatively stable around 17.9 ± 0.07 °C between January 2016 and January 2017, after which time it increased gradually to 18.6 °C by April 2017. At the time of our visit (October 2017), a spot measurement using a portable electronic temperature sensor was 20.7 °C near the stalagmite site. The stable relative humidity suggests that drip-water evaporation should be minimal but that temperature variations, if present in the past, may have had a small influence on $\delta^{18}O_c$ of ~0.2‰ VPDB per degree Celsius.

The isotope-enabled transient simulation iTRACE data (Extended Data Figs. 3–5) show differences in precipitation rate, $\delta^{18}O_p$, wind field (600 hPa) and $\delta^{18}O$ of water vapour at the Early Holocene (11 ka) relative to 14 ka. The core NAM region is defined as between 18° and 33° N and 112° and 102° W. The hydroclimate simulations of iCESM, which is the model used for the iTRACE experiments, have been validated against present-day observations both on a global scale[57] and specifically in North America[58].

We also measured speleothem $\delta^{13}C$ values. Speleothem $\delta^{13}C$ is potentially related to the proportion of soil biogenic production and bedrock carbon in dissolved inorganic carbon, water residence times in soils during which they can become charged with biogenic carbon (with low $\delta^{13}C$ values), changing vegetation type (lower $\delta^{13}C$ values associated with more C3 vegetation and higher with C4 vegetation), changing $\delta^{13}C$ values of vegetation related to moisture stress or kinetic isotopic effects associated with previous calcite precipitation in the epikarst[59]. It is challenging to isolate a single dominant control on speleothem $\delta^{13}C$ values without replication or more detailed studies. However, we suspect that GC-1 $\delta^{13}C$ is related to the $\delta^{13}C$ value of vegetation over the cave site, which in turn may reflect either changes in the proportion of C4 plants (higher $\delta^{13}C$) relative to C3 plants (lower $\delta^{13}C$) or simply changes in the average vegetation $\delta^{13}C$ value itself. To test the latter possibility, we compared GC-1 $\delta^{13}C$ with a radiocarbon-dated record of insect chitin recovered from bat guano in the Grand Canyon[60]. Insect chitin is related to the diet of the insects who feed on the plants. The two records are similar: generally low but variable $\delta^{13}C$ values between ~11,000 and 14,000 yr B2k, with a transition to higher $\delta^{13}C$ values in the Early Holocene for both speleothem and insect chitin $\delta^{13}C$ values (Extended Data Fig. 6). This positive covariation suggests that the speleothem $\delta^{13}C$ values are controlled, at least in part, by the $\delta^{13}C$ values of vegetation in the Grand Canyon.

Data availability

The GC-1 $\delta^{18}O_c$, $\delta^{13}C$ and U-series data are archived with the NOAA Paleoclimatology Program at https://www.ncei.noaa.gov/access/paleo-search/study/38391.

Code availability

The iTRACE outputs used in this study can be downloaded from the NCAR Climate Data Gateway (https://www.earthsystemgrid.org/

dataset/ucar.cgd.ccsm4.iTRACE.html; https://doi.org/10.26024/b290-an76). iTRACE 1.3 is performed in iCESM 1.3. The iCESM 1.3 code is publicly accessible via GitHub (https://github.com/NCAR/iCESM1.3_iHESP_hires).

References

52. Hill, C. A. & Polyak, V. J. Karst hydrology of Grand Canyon, Arizona, USA. *J. Hydrol.* **390**, 169–181 (2010).
53. Tobin, B. W., Springer, A. E., Ballensky, J. & Armstrong, A. Cave and karst of the Grand Canyon World Heritage Site. *Z. Geomorphol.* **62**, 125–144 (2021).
54. Heimel, S. M. & Tobin, B. W. Geospatial applications of cave resource data to better understand epikarst and unsaturated zone groundwater flow path development. *Geosciences* **12**, 1–12 (2022).
55. Cheng, H. et al. Improvements in ^{230}Th dating, ^{230}Th and ^{234}U half-life values, and U–Th isotopic measurements by multi-collector inductively coupled plasma mass spectrometry. *Earth Planet. Sci. Lett.* **371–372**, 82–91 (2013).
56. Breitenbach, S. F. M. et al. Constructing proxy records from age models (COPRA). *Climate* **8**, 1765–1779 (2012).
57. Brady, E. et al. The connected isotopic water cycle in the Community Earth System Model Version 1. *J. Adv. Model. Earth Syst.* **11**, 2547–2566 (2019).
58. Fu, M. Revisiting Western United States hydroclimate during the last deglaciation. *Geophys. Res. Lett.* **50**, e2022GL101997 (2023).
59. Fohlmeister, J. et al. Main controls on the stable carbon isotope composition of speleothems. *Geochim. Cosmochim. Acta* **279**, 67–87 (2020).
60. Wurster, C. M. et al. Stable carbon and hydrogen isotopes from bat guano in the Grand Canyon, USA, reveal Younger Dryas and 8.2 ka events. *Geology* **36**, 683 (2008).

Acknowledgements

We thank L. Sangaila for field assistance. G. Lucia drilled some of the U-series powders. We thank the National Park Service for permission to complete research completed under permit GRCA-2017-SCI-0055. Cave-water samples at Cave 3504 in Parashant National Monument were collected under permit PARA-2014-SCI-0001. The National Science Foundation provided funding through ATM-1405546 to UNLV and 1405557 to UNM, and for laboratory facilities through grants EAR 0521196 to UNLV and EAR 0326902 and ATM 0703353 to UNM.

Author contributions

Fieldwork and site selection were done by M.S.L. and B.W.T. M.S.L. completed all stable-isotope analyses and Y.A. and V.J.P. completed age dating. Model analysis was completed by S.G.D. and X.D. M.S.L. wrote the manuscript and completed the data analysis, with contributions from X.D., S.G.D., B.W.T., Y.A. and V.J.P. All authors contributed to finalizing and approving the manuscript.

Competing interests

The authors declare no competing interests.

Additional information

Extended data is available for this paper at https://doi.org/10.1038/s41561-023-01272-6.

Supplementary information The online version contains supplementary material available at https://doi.org/10.1038/s41561-023-01272-6.

Correspondence and requests for materials should be addressed to Matthew S. Lachniet.

Peer review information *Nature Geoscience* thanks Gabriel Bowen, Kim Beisner and the other, anonymous, reviewer(s) for their contribution to the peer review of this work. Primary Handling Editor: James Super, in collaboration with the *Nature Geoscience* team.

https://doi.org/10.1038/s41561-023-01272-6

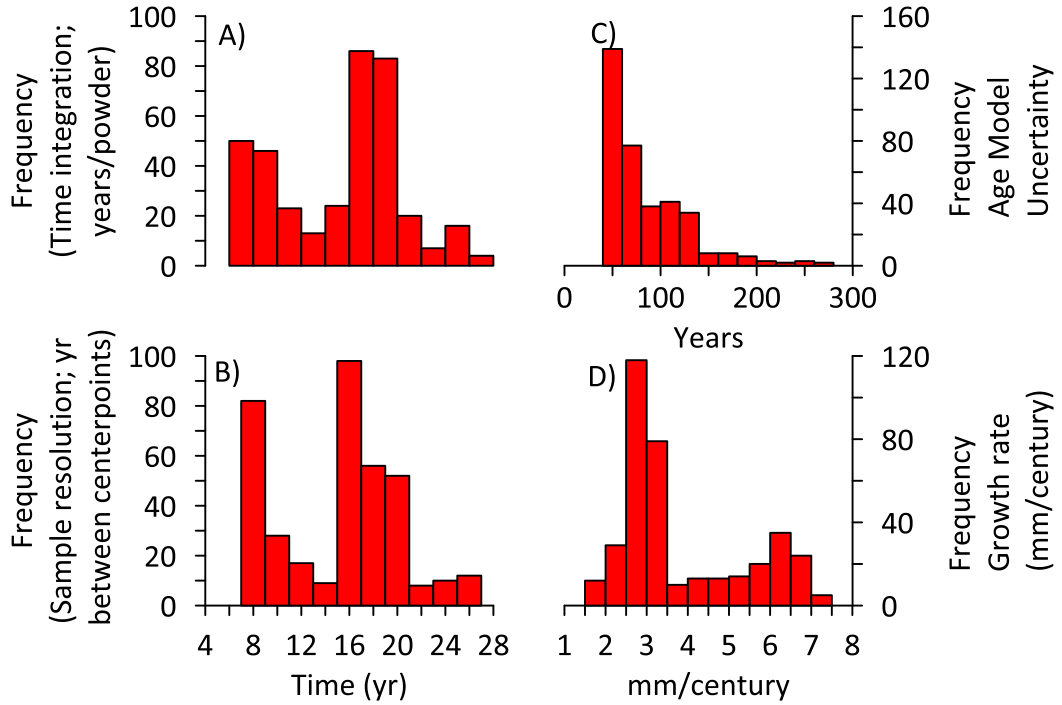

Extended Data Fig. 1 | Grand Canyon stalagmite (GC-1) age model metadata. Histograms show the frequency of observations for **a**) years represented by each sample, **b**) years between the center points of each sample, on the same x-axis as A), **c**) frequency of age model uncertainties due to time-varying growth rates and chronological age precision, and **d**) frequency of growth rate variations. The stalagmite $\delta^{18}O$ and $\delta^{13}C$ resolution is at the decadal to bi-decadal time scale, with an age model uncertainty between ~50 and 150 years. Most of the stalagmite grew between 2-3 mm per century, with a period of faster growth of 5-6 mm per century between 11,600 and 10,300 yr B2k.

https://doi.org/10.1038/s41561-023-01272-6

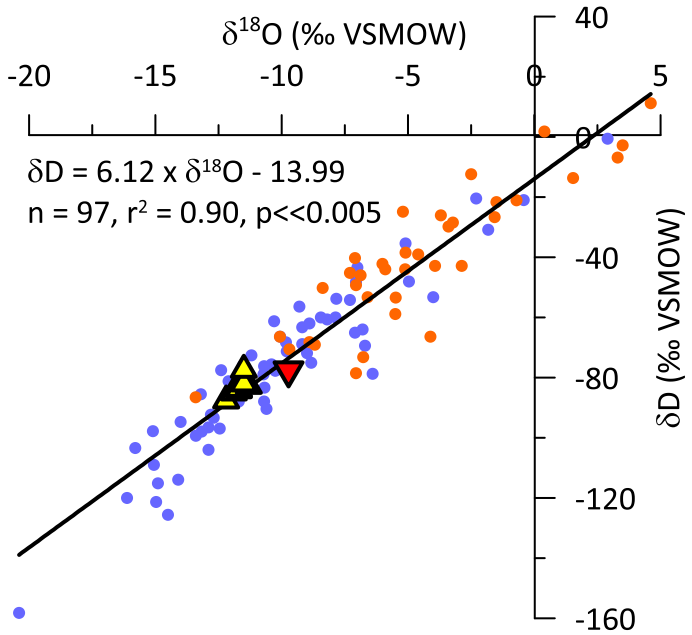

Extended Data Fig. 2 | Meteoric water line for Flagstaff, AZ. Winter precipitation (NDJFMAM) are blue circles, and summer (JJASON) are orange. Cave waters (solid triangles) plot close to the Flagstaff meteoric water line and are most consistent with winter season infiltration.

https://doi.org/10.1038/s41561-023-01272-6

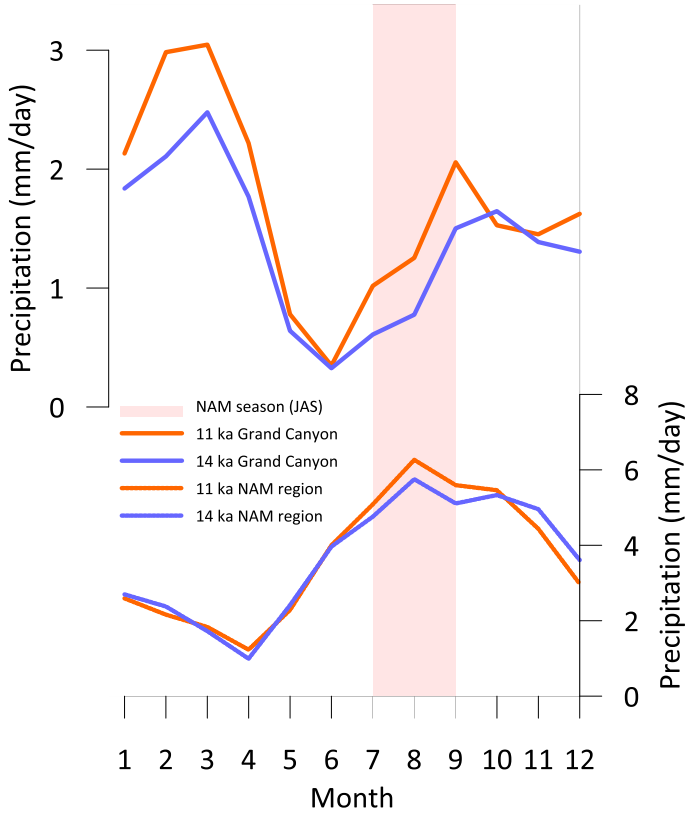

Extended Data Fig. 3 | Simulated North American Monsoon monthly precipitation at Grand Canyon and the core NAM region. Top shows that iTRACE simulates the bimodal seasonal cycle at Grand Canyon (see text Fig. 3), with a rainfall minimum in June. Further, the NAM summer rainfall is stronger at 11 ka than at 14 ka at Grand Canyon, consistent with the rise in $\delta^{18}O_c$ and $\delta^{234}U_i$ evidence of increasing effective moisture. Winter season rainfall rate also increased with a small rise in $\delta^{18}O_p$ (see Extended Data Figure 5).

https://doi.org/10.1038/s41561-023-01272-6

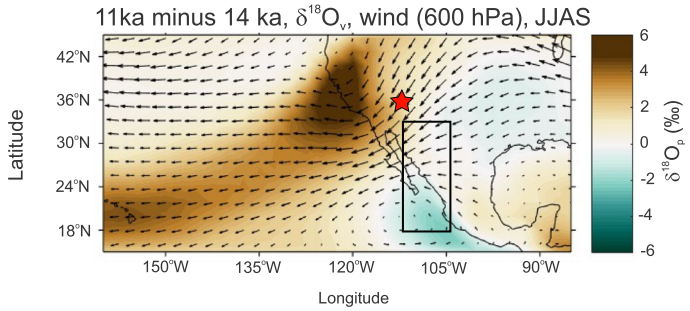

Extended Data Fig. 4 | Simulated wind field evolution and $\delta^{18}O$ of water vapor at 11ka relative to 14 ka. The anomaly difference in wind field and $\delta^{18}O$ of water vapor shows a weakening of the polar jet (weaker westerlies) at 11 ka relative to 14 ka and an increase in summer (JJAS) water vapor $\delta^{18}O$. Box shows the 'core' NAM region; red star is Grand Canyon.

https://doi.org/10.1038/s41561-023-01272-6

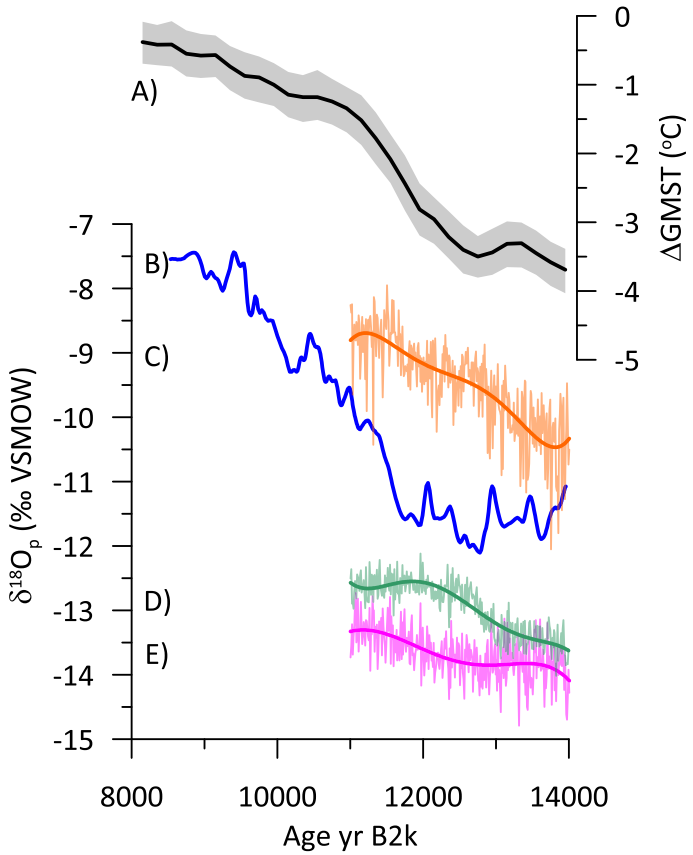

Extended Data Fig. 5 | Comparison between GC-1 estimated $\delta^{18}O_p$, global mean surface temperature (GMST), and iTRACE seasonal $\delta^{18}O_p$. a) is the GMST record of Ref. 40 showing the deglacial rise in temperature; grey envelope is 10 and 90% percentiles; **b**) is stalagmite GC-1 estimated as $\delta^{18}O_p$ on the VSMOW scale, using the GMST record and the water-calcite fractionation equation of Ref. 29, **c**) through E) are $\delta^{18}O_p$ for JJA, mean annual, and DJF seasons from the iTRACE simulation. The steep rise in GC-1 estimated $\delta^{18}O_p$ at 11 ka closer to the summer $\delta^{18}O_p$ end-member value suggests that summer monsoon moisture was an increasing proportion of total infiltration at 11 ka relative to 14 ka, evidence supportive of an Early Holocene NAM strengthening.

https://doi.org/10.1038/s41561-023-01272-6

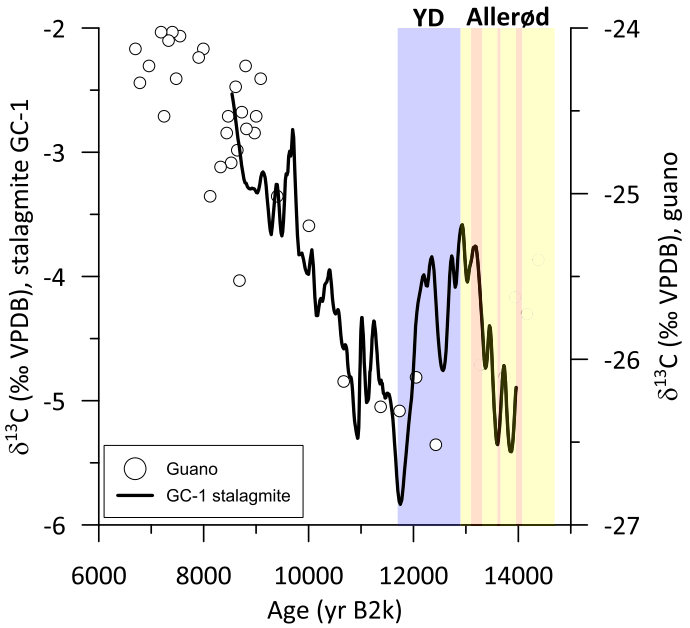

Extended Data Fig. 6 | Covarying Grand Canyon stalagmite and vegetation carbon isotope values. Comparison of speleothem GC-1 $\delta^{13}C$ COPRA modeled proxy data (left axis, solid black line) and bat guano-derived insect chitin $\delta^{13}C$ values (right axis, open circles; Ref. 57) from the Grand Canyon suggests that changing speleothem $\delta^{13}C$ was related to a change in $\delta^{13}C$ value of vegetation. Vertical bars are the YD and Greenland interstadial events GS-1a-e.